Synthesis of Long-Period Surface Waves and Its Application to Earthquake Source Studies—Kurile Islands Earthquake of October 13, 1963

HIROO KANAMORI[1]

Department of Earth and Planetary Sciences
Massachusetts Institute of Technology
Cambridge, Massachusetts 02139

Normal mode solutions for a spherical earth model are superposed to obtain realistic synthetic surface waves for various force systems. The calculation of excitation functions is greatly facilitated by the variational technique. The effects of attenuation and instrument response are included in the synthesis. The synthesized seismograms are compared with the actual seismograms for wave form, amplitude, radiation pattern, and phase to obtain various source parameters such as force geometry, source-time function, seismic moment, source dimension, and rupture velocity. The application is made to the Kurile Island earthquake of October 13, 1963 ($M = 8.3$). The comparison is made for Love waves G_4 and Rayleigh waves R_4 for a period range 100 to 400 sec. It is found that a reverse dip-slip fault with a dip angle of 22° and a dip direction of N47°W can explain the observation reasonably well. Other parameters determined are as follows: seismic moment, 7.5×10^{29} dyne-cm; source-time function, step function; fault length, 200 to 300 km; rupture velocity, 2.7 to 4.5 km/sec in the direction N43°E.

The amplitude and phase spectra of earthquake surface waves have been successfully used for estimating various source parameters such as force geometry [e.g. *Brune et al.*, 1960; *Aki*, 1960*a*, *b*; *Brune*, 1961; *Wu and Ben-Menahem*, 1965], fault length, rupture velocity [e.g. *Benioff et al.*, 1961; *Press et al.*, 1961; *Ben-Menahem and Toksöz*, 1962], source-time function [e.g. *Ben-Menahem and Toksöz*, 1963*a*, *b*], and dislocation [*Aki*, 1966*a*, *b*; *Tsai and Aki*, 1969].

With the recent developments of the theory of the excitation of surface waves [*Alterman et al.*, 1959; *Haskell*, 1963, 1964; *Ben-Menahem and Harkrider*, 1964; *Saito*, 1967], it is now possible to use more elaborate techniques in source studies. For example, we can calculate theoretical surface wave trains, excited by an arbitrary source, for a radially heterogeneous earth model. These synthetic seismograms can be directly compared with observed seismograms to make a most straightforward determination of source parameters.

Synthetic seismograms of surface waves have been studied by *Lamb* [1904], *Jobert* [1962], *Satô and Usami* [1962], *Satô et al.* [1967, 1968] and *Usami et al.* [1965]. However, no extensive application has been made to the interpretation of observed seismograms. This paper describes a procedure of calculating most realistic synthetic seismograms and its application to the determination of various source parameters of the Kurile Islands earthquake of October 13, 1963 ($M = 8.3$). The hypocenter data are: origin time, 05h 17m 57s; latitude, 44.8°N; longitude, 149.5°E; depth, 60 km. We shall first present the seismograms of this earthquake.

DATA

The actual-size copies of the long-period seismograms from all the worldwide standard stations (WWSSN) of the United States Coast and Geodetic Survey (USCGS) were collected. At many stations multiple Rayleigh waves R_4 and Love waves G_4 were on scale and could be clearly identified. We used vertical components for Rayleigh waves, and horizontal components for Love waves. Wherever necessary, transverse components synthesized from two horizontal components were used to obtain Love waves.

[1] On leave from the Earthquake Research Institute, University of Tokyo, Japan.

Otherwise, Love wave trains obtained from a single component were multiplied by an appropriate factor to convert them to transverse components. Rayleigh waves were windowed between group velocities of 3.90 and 3.47 km/sec, and Love waves between 4.3 and 4.5 km/sec. The seismograms were then digitized at every 4 sec. Table 1 lists the stations and other pertinent data used here.

All the seismograms were equalized to a distance of $\pi/2$, which corresponds to a propagation distance of $7\pi/2$ for R_4 and G_4. The magnification was equalized to 1500. For the equalization of distance, we Fourier-analyzed the seismograms u (Δ, t) at a propagation distance Δ to obtain the complex spectrum U (Δ, ω). Then, as a propagating wave on a sphere, the equalized seismogram at distance Δ_0 (here $\Delta_0 = 7\pi/2$) can be obtained as

$$u(\Delta_0, t) = \left(\left|\frac{\sin \Delta}{\sin \Delta_0}\right|\right)^{1/2} \int_{-\infty}^{+\infty} U(\Delta, \omega) \exp\left\{i\left[\omega\left(\frac{\Delta - \Delta_0}{C}\right) - \frac{\pi}{2} M\right]\right\} \cdot e^{k^*(\Delta - \Delta_0)} \cdot e^{i\omega t}\, d\omega$$

where C and k^* are phase velocity and attenuation coefficient as a function of frequency, and M is the number of polar or antipolar passages in going from Δ to Δ_0. Since the equalization made here involves no polar or antipolar passages, M is equal to 0. The values of k^* and C used for the equalization are given in Tables 2 and 3 as functions of the period from 100 to 400 sec. Most of these values are taken from *Kanamori* [1970] and represent the average values for a number of great circle paths. Since the equalization is made for relatively small

TABLE 1. Station Data

Station	Δ, deg	l, km	$l + L$, km	ϕ, deg	ϕ', deg	Component	Magnification
AAE	98.021	10898.3	40038.8	291.1	42.3	Z, NS, EW	750
ADE	79.986	8900.7	40009.9	189.0	7.8	Z, EW	750
AFI	68.178	7586.7	40023.5	139.1	331.3	Z, NS, EW	750
BAG	37.319	4150.8	40028.8	230.0	34.6	Z, EW	1500
BEC	97.136	10787.5	40016.9	28.6	336.2	Z, EW	1500
BKS	63.492	7054.8	40035.7	62.1	307.3	NS	3000
CAR	115.863	12874.8	40023.5	40.5	332.0	Z	3000
CTA	64.631	7192.5	40009.2	183.4	2.6	EW	3000
GDH	65.007	7215.2	40009.9	8.9	342.1	Z, EW	750
GOL	72.343	8036.4	40029.9	51.4	313.8	Z, EW	1500
HKC	36.594	4069.4	40036.4	243.9	43.7	Z, NS	1500
HNR	54.791	6097.1	40010.7	167.4	350.9	Z, EW	1500
IST	79.293	8806.7	40024.1	318.5	38.6	Z, NS, EW	1500 (Z) 750 (NS, EW)
KIP	48.781	5424.1	40041.9	100.7	311.3	NS	750
KTG	64.939	7207.5	40009.2	356.8	6.7	Z, EW	1500
LPA	156.835	17445.2	40040.7	74.3	303.5	Z	750
MAN	38.490	4281.2	40027.5	227.7	33.0	NS	750
MDS	77.582	8616.1	40023.1	39.9	321.2	EW	1500
MUN	81.430	9061.5	40016.7	208.4	23.3	Z, EW	750
NAI	106.868	11884.9	40040.8	285.5	43.4	NS, EW	1500
NDI	58.290	6479.4	40042.1	280.3	52.9	Z	1500
NUR	65.868	7312.4	40015.8	333.6	39.8	EW	3000
PRE	129.529	14410.3	40043.1	271.6	52.1	Z, NS	1500
RAB	48.821	5432.5	40009.2	176.5	357.5	EW	750
SBA	122.832	6345.2	40009.2	175.7	345.4	Z	750
SHI	73.996	8223.2	40036.6	296.1	47.4	Z, NS	1500
TOL	92 416	10260.8	40013.1	339.9	18.5	Z, EW	1500
TUC	74.235	8249.0	40034.7	60.2	313.2	Z, NS	1500

Definitions.
Δ is distance; l, minor arc; $l + L$, length of great circle; ϕ, azimuth; ϕ', back azimuth.

distances (maximum 67°, minimum 2.4°, average 27° see Table 1), use of any other reasonable values of C and k^* does not significantly alter the equalized waveform.

The equalized seismograms are shown in Figures 1 and 2 with the three-letter station abbreviations used by USCGS. In Figures 1 and 2, the starting time is the same for all the traces; the Rayleigh wave trains start at 10h 30m 30s and the Love wave trains at 9h 36m. The difference in the group arrival times from one station to another reflects the regional variation of the structure. For Rayleigh waves, upward motion is taken positive (upward on the trace), and for Love waves, counter-clockwise motion around the source is taken positive (upward on the trace). The circular plots at the center of these figures show the maximum amplitude of the trace. Three important features immediately show up in the equalized seismograms: (1) the maximum amplitude is slightly larger for Love waves than for Rayleigh waves; (2) the radiation pattern is nearly two-lobed for Rayleigh waves and four-lobed for Love waves; (3) the radiation pattern is asymmetric for both Love and Rayleigh waves and the amplitude is larger in the northeast direction than in the southwest direction. We shall explain these features on the basis of synthetic seismograms.

We believe that this way of presenting seismograms is most suitable for visualizing the over-all nature of radiation and therefore the source mechanism of great earthquakes.

Synthetic Seismogram

For the computation of synthetic seismograms we used the results of *Saito* [1967], who introduced a variational technique in the calculation of the residue contributions from Rayleigh and Love poles. Since the details are given in Saito's paper, the method will be briefly outlined in the following.

TABLE 2. Period T, Phase Velocity C, Q, and Attenuation Coefficient k^* for Rayleigh Waves

T, sec	C, km/sec	Q	$10^5 \times k^*$, km^{-1}
406	5.970	250	0.70
350	5.620	220	1.02
325	5.464	182	1.41
300	5.292	183	1.54
275	5.106	185	1.70
250	4.916	189	1.85
225	4.739	179	2.18
200	4.575	171	2.56
175	4.432	147	3.37
150	4.296	130	4.40
125	4.196	130	5.21
100	4.100	130	6.28

TABLE 3. Period T, Phase Velocity C, Q, and Attenuation Coefficient k^* for Love Waves

T, sec	C, km/sec	Q	$10^5 \times k^*$, km^{-1}
410	5.582	130	1.31
350	5.395	120	1.69
325	5.317	108	2.03
300	5.230	110	2.16
275	5.150	116	2.23
250	5.072	112	2.55
225	4.995	113	2.81
200	4.923	111	3.22
175	4.849	122	3.35
150	4.780	117	4.09
125	4.715	119	4.91
100	4.642	100	7.31

We take the polar coordinate (r, θ, ϕ) with the origin at the center of the earth. From Saito's equation 46, the transverse component of the torsional oscillation (Love wave) $U_\phi(r, \theta, \phi, t)$, owing to a point source placed at $r = r_s$ and changing stepwise in time at $t = 0$, can be written as

$$U_\phi(r, \theta, \phi, t) = \sum_{n=0}^{\infty} \frac{y_{1,n}(r)}{\sigma_n^2 I_{1,n}} \cos \sigma_n t \sum_{m=0}^{n} \left(-\frac{\partial P_n^m(\cos\theta)}{\partial \theta} \right) \cdot (A_m^c \cos m\phi + A_m^s \sin m\phi)$$

$$A_m^c = r_s^2 (f_{2,m}^c y_{1,n}(r_s) - f_{1,m}^c y_{2,n}(r_s)) \qquad (1)$$

$$A_m^s = r_s^2 (f_{2,m}^s y_{1,n}(r_s) - f_{1,m}^s y_{2,n}(r_s))$$

where $y_{1,n}(r)$ and $y_{2,n}(r)$ represent the radial factors of displacement and stress of a normal mode of order n respectively, and where σ_n is the eigen angular frequency. The quantity $I_{1,n}$ is an energy integral defined by

$$I_{1,n} = \int_0^a \rho(r) r^2 y_{1,n}^2(r)\, dr$$

where a is the earth's radius and $\rho(r)$ is the density as a function of r. The quantities $r_s^2 f_{1,m}^c$, $r_s^2 f_{1,m}^s$, $r_s^2 f_{2,m}^c$, and $r_s^2 f_{2,m}^s$ are determined by the geometry of the force system at the source. For a unit single force, a single couple with unit moment and a double couple with unit

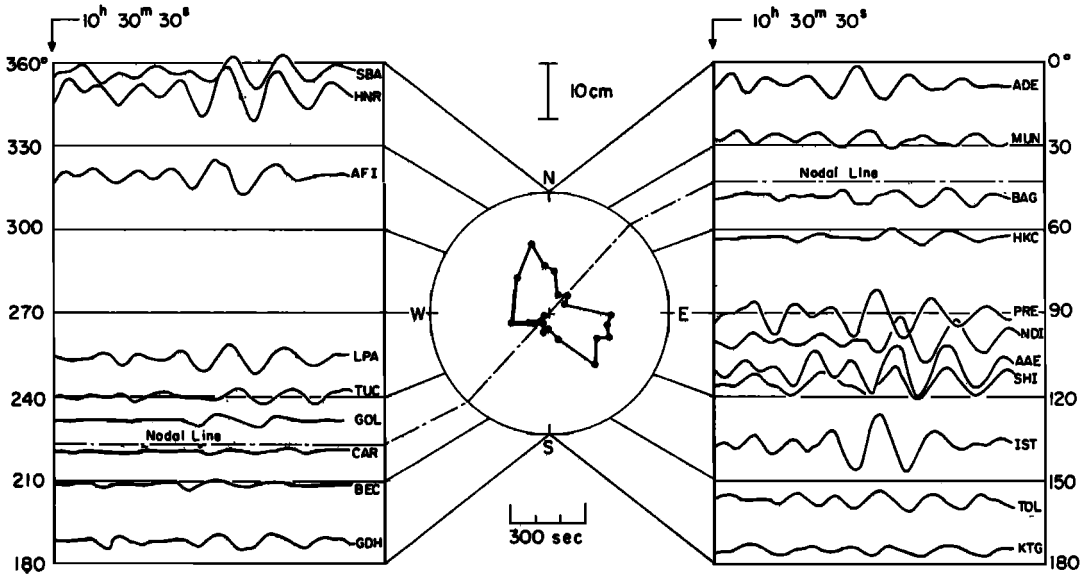

Fig. 1. Equalized Rayleigh waves ($R4$) for the Kurile Islands earthquake of October 13, 1963. All the seismograms are equalized to a distance of $\pi/2$ (propagation distance of $7\pi/2$). The vertical scale gives the trace amplitude on the standard 30–100 long-period seismograms with a magnification of 1500.

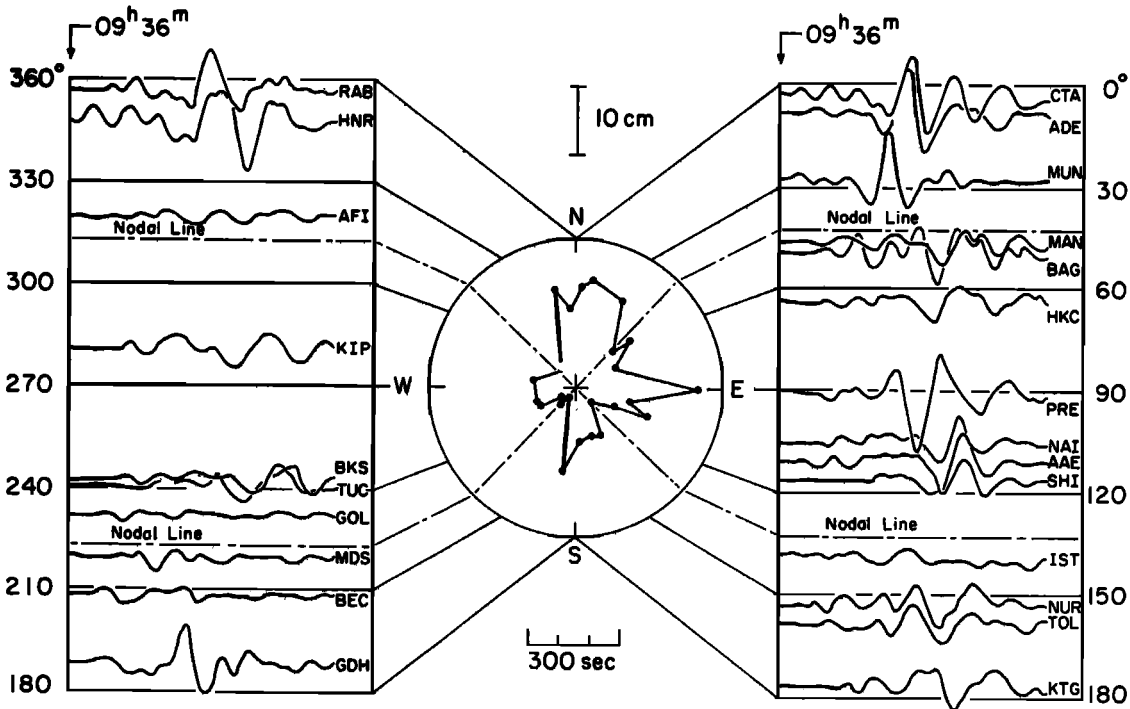

Fig. 2. Equalized Love waves ($G4$) for the Kurile Islands earthquake of October 13, 1963. (For explanations, see the caption for Figure 1.)

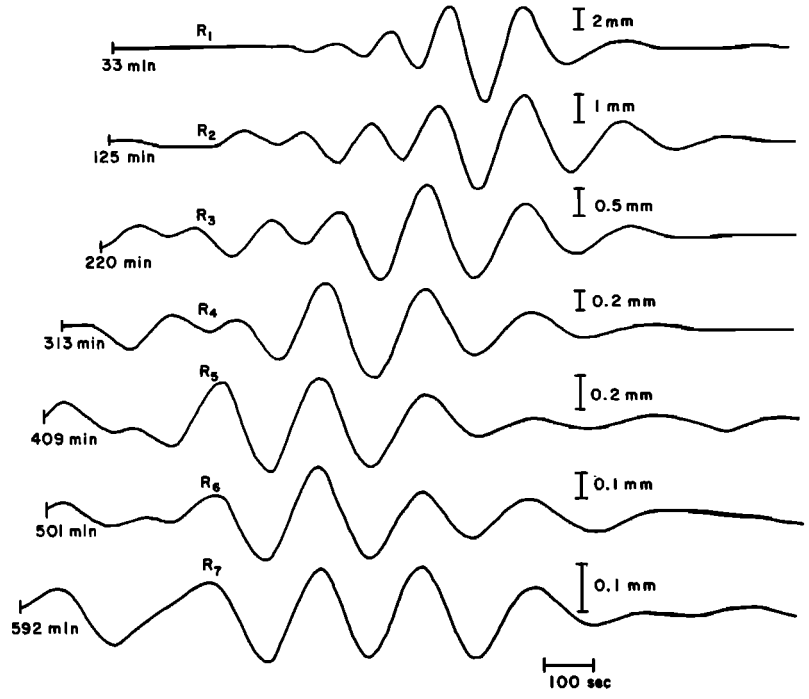

Fig. 3. Synthetic Rayleigh waves at $\Delta = 90°$ and $\phi = 90°$ for a double couple 45° dip-slip source varying stepwise in time. The seismic moment is 5×10^{26} dyne-cm. The times given at the beginning of each trace are the times after the origin time. The vertical scale gives the trace amplitude on the standard 30–100 seismograph records with a magnification of 1500.

moment, the expressions have been given by equations 58, 60, and 61 of *Saito* [1967]. In those equations, the force is specified by a unit vector **v** parallel to the force. For couples, the direction of the arm is given by a unit vector **n**. The components of **v** and **n** in Cartesian coordinates taken at the source, z axis coinciding with the polar axis, specify the force system completely. For example, a simple left-lateral vertical strike-slip fault whose strike coincides with the y axis can be represented by **v** (0, 1, 0) and **n** (1, 0, 0), and a reverse pure dip-slip fault whose strike is parallel to the y axis can be represented by **v** ($-\cos\delta$, 0, $\sin\delta$) and **n** ($\sin\delta$, 0, $\cos\delta$), where δ is the dip angle measured from the x axis. In (1) the summation for n extends over fundamental and higher modes. However, for surface waves at large distances from shallow focus earthquakes, only the contributions from the fundamental modes are important [e.g. *Usami et al.*, 1965]. The vertical component U_r always vanishes, and the radial component U_θ is, for large n, much smaller than U_ϕ.

For spheroidal oscillations (Rayleigh waves) from equation 47 of *Saito* [1967], the vertical component U_r can be written, for a step excitation, as

$$U_r(r, \theta, \phi, t) = \sum_n \frac{y_{1,n}(r)}{\sigma_n^2(I_{1,n} + N^2 I_{2,n})} \cos \sigma_n t \cdot \sum_{m=0}^{n} P_n^m(\cos\theta) \cdot (A_m^c \cos m\phi + A_m^s \sin m\phi)$$

$$N^2 = n(n+1)$$

$$A_m^c = r_s^2[(y_{1,n}(r_s) f_{2,m}^c - y_{2,n}(r_s) f_{1,m}^c) + N^2(y_{3,n}(r_s) f_{4,m}^c - y_{4,n}(r_s) f_{3,m}^c)] \quad (2)$$

$$A_m^s = r_s^2[(y_{1,n}(r_s) f_{2,m}^s - y_{2,n}(r_s) f_{1,m}^s) + N^2(y_{3,n}(r_s) f_{4,m}^s - y_{4,n}(r_s) f_{3,m}^s)]$$

where $y_{1,n}$ and $y_{3,n}$ represent radial factors of displacements, and $y_{2,n}$ and $y_{4,n}'$ the radial factors of stresses. As before,

$$I_{1,n} = \int_0^a \rho(r) r^2 y_{1,n}^2(r)\, dr$$

$$I_{2,n} = \int_0^a \rho(r) r^2 y_{3,n}^2(r)\, dr$$

The quantities $r_s^2 f_{1,m}^c$, $r_s^2 f_{1,m}^s$, and so on, which can be determined, once the force system is specified in terms of **n** and **v**, have been given by equations 58, 60, and 61 of *Saito* [1967].

The quantities $y_{i,n}'s$, $I_{i,n}'s$, and $\sigma_n's$ can be easily calculated by a standard technique that incorporates numerical integrations of vibration equations for a radially heterogeneous, self-gravitating sphere [*Takeuchi et al.*, 1962; *Bolt and Dorman*, 1961]. A computer program written by *Kanamori and Abe* [1968] was used here. Since the spectrums of R_4 and G_4 are limited to a range from 100 to 400 sec, we computed all the fundamental modes from $n = 15$ ($T = 450$ sec for Love waves and $T = 425$ sec for Rayleigh waves) to $n = 100$ ($T = 86$ sec for Love waves and $T = 97$ sec for Rayleigh waves). For $n \geq 51$ the effect of gravity was ignored in the calculation of Rayleigh waves.

For a meaningful comparison between observed and synthetic seismograms, appropriate selection of an earth model to be used in the calculation of synthetic seismograms is crucial. In the present study we used model 5.08 M, which was derived, on the basis of group velocity data, from the 27 models presented by *Press* [1970]. (For details, see *Kanamori* [1970]). This model fits the average observed phase-velocity data to within $\pm 0.15\%$ and $\pm 0.2\%$ for Rayleigh and Love waves, respectively.

For direct comparison of the synthetic seismograms with the observed seismograms, the effect of attenuation and instrument response must be included. The effect of attenuation was included by multiplying each term of equations 1 and 2 by a factor $\exp(-\sigma_n t/2Q)$ where Q is the quality factor as a function of period. The values of Q given in Tables 2 and 3 were used.

The instrument response was included on frequency domain: the equations 1 or 2 multiplied by $\exp[-\sigma_n t/2Q]$ was Fourier-transformed, multiplied by the instrument response

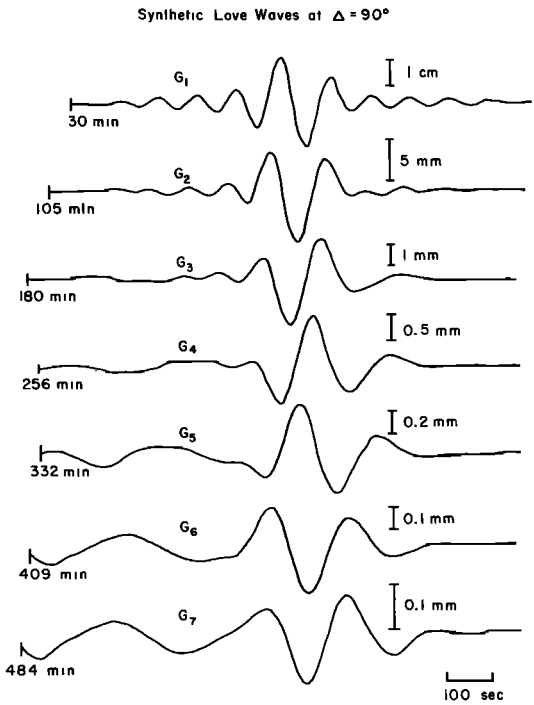

Fig. 4. Synthetic Love waves at $\Delta = 90°$ and $\phi = 45°$ for a double-couple 45° dip-slip source varying stepwise in time. (For explanations, see the caption for Figure 3.)

calculated by the formula of *Hagiwara* [1958], and then inverse-transformed back to time domain. For purposes of calculation, the parameters in Hagiwara's formula are assumed to be T_p (pendulum period) = 30 sec, T_g (galvanometer period) = 100 sec, hp (damping constant of pendulum) = 1, hg (damping constant of galvanometer) = 1, σ^2 (coupling factor) = 0.1, and magnification = 1500. The convention for the phase noted by *Brune* [1962] was observed. Unless otherwise stated, synthetic seismograms that appear in this paper are for a unit couple with a moment of 5×10^{26} dyne-cm. The focal depth of the Kurile Islands earthquake has been determined at about 60 km by the USCGS. Since the radiation of long-period waves is not very sensitive to the focal depth, we assumed the focal depth at 53 km.

We shall compare the synthetic seismograms thus calculated with the observed seismograms in terms of wave form, relative excitation between Love and Rayleigh waves, and radiation pattern.

Wave form. The wave form of the synthetic seismogram was found not to be very sensitive to the force geometry. We shall therefore use an arbitrary source, a double-couple dip-slip with $\delta = 45°$, for comparison of wave form. Figures 3 and 4 show, respectively, the synthetic multiple Rayleigh and Love waves at $\Delta = \pi/2$. The dispersion and attenuation are clearly demonstrated. Figure 5 compares synthetic Rayleigh waves, R_3, R_4, and R_5 at $\Delta = 98°$ with observed multiple Rayleigh waves R_3, R_4, and R_5 at $AAE(\Delta = 98°)$. The amplitude and the group arrival time are arbitrary. It is seen that the synthetic seismograms can explain the nature of the observed seismograms very well, even to details. This suggests that the earth model used here and the step-wise source function are appropriate. Figure 6 shows a similar comparison for Love waves. The agreement between the synthetic and observed seismograms is reasonably good but not as good as for Rayleigh waves. This is probably due to the effect of lateral heterogeneity of the earth, which is larger on Love waves than on Rayleigh waves [*Kanamori*, 1970].

Relative excitation. The excitation of Rayleigh waves relative to Love waves depends on the source geometry. For a guideline to estimate the source geometry from the relative excitation between Love and Rayleigh waves, the maximum amplitude of G_4 and R_4 has been calculated for eight fundamental source geometries, as shown in Figure 7. The source system designated as 45° strike slip is a pure strike slip with fault planes dipping 45°. The 45° dip-slip is a pure dip-slip with a dip angle of 45°. As seen in Figure 7, the relative excitation is sufficiently different to discriminate source geometries.

Radiation pattern. The radiation pattern of surface waves varies with period and is therefore difficult to represent in a straightforward manner. However, in view of the striking similarity between the synthetic and observed seismograms, it seems most reasonable to use the maximum trace amplitude to represent the

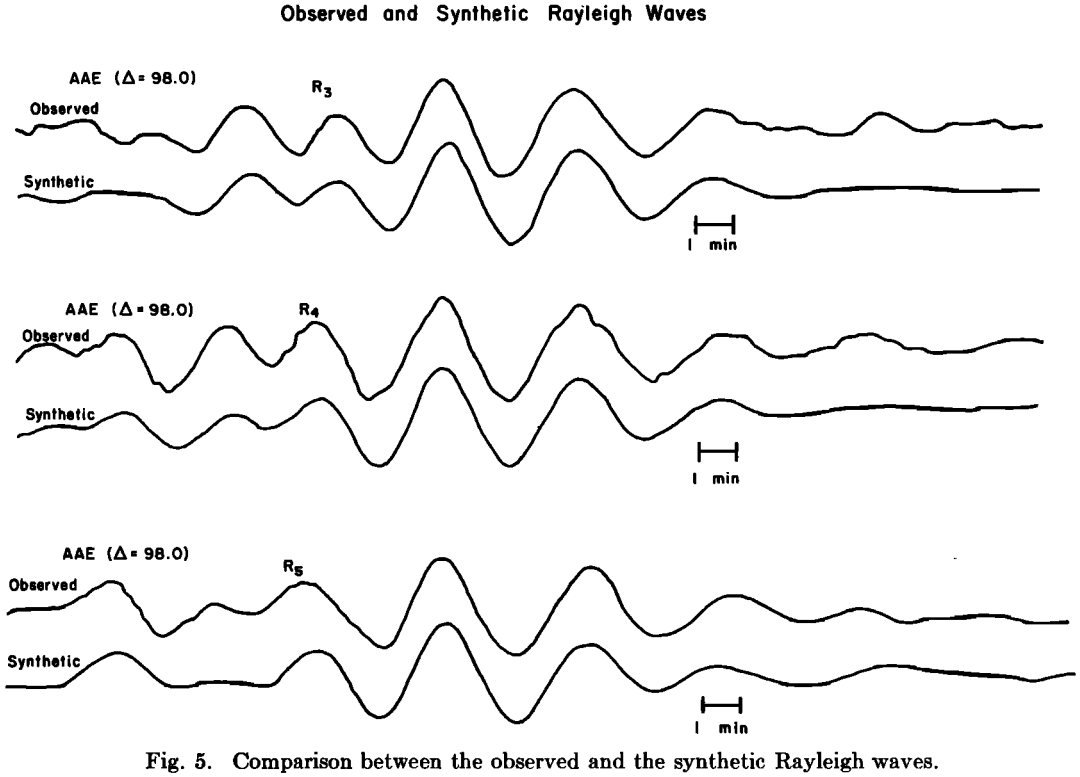

Fig. 5. Comparison between the observed and the synthetic Rayleigh waves.

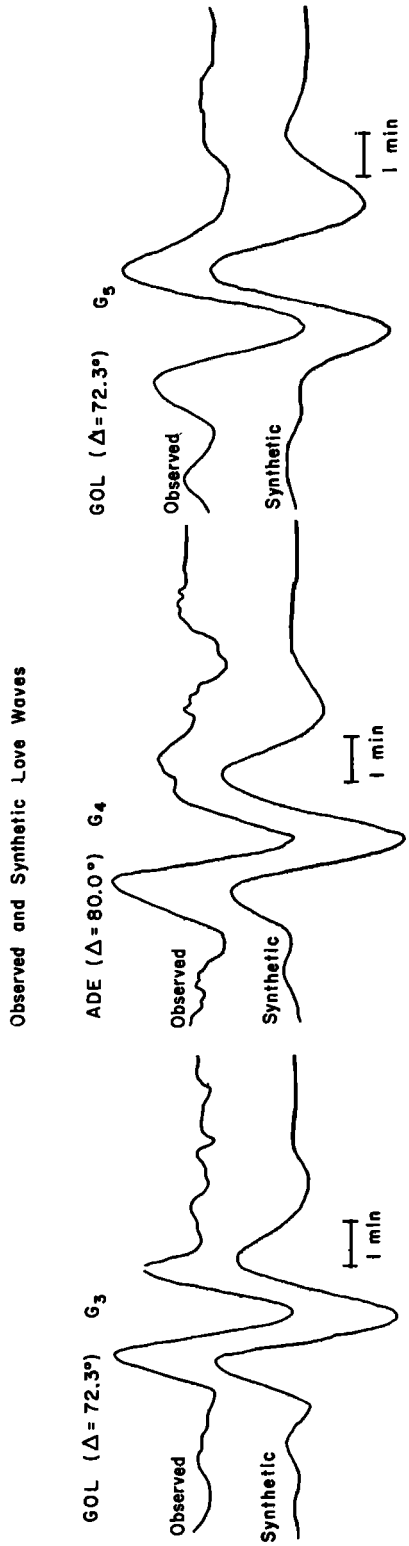

Fig. 6. Comparison between the observed and the synthetic Love waves.

radiation pattern of surface waves. Figure 7 shows the maximum amplitude radiation patterns of G_4 and R_4 for the eight fundamental source geometries. The radiation pattern is very sensitive to the source geometry. The radiation patterns for multiple surface waves other than R_4 and G_4 can be easily estimated from Figure 7 by using Figures 3 and 4 to correct for the attenuation.

Interpretation

Relative excitation and radiation pattern. Comparison of Figures 1 and 2 with Figure 7 immediately leads to the conclusion that, among the eight fundamental source geometries, only the double-couple 45° dip-slip source is consistent with the observation; the maximum amplitude of Love waves is slightly larger than that of Rayleigh waves, and the radiation pattern is four-lobed for Love waves and two-lobed for Rayleigh waves. The strike of the fault plane should coincide with the nodal direction of the observed radiation patterns (NE–SW). From the surface-wave data alone, however, it is difficult to constrain the dip angle within a narrow range. For example, a change of the dip angle from 45° to 20° does not greatly affect the relative excitation and the radiation pattern; the synthetic seismograms for 20° dip slip are still consistent with the observations. Further, there remains the possibility that the source has some strike-slip component. From the surface-wave data alone, we can only conclude that the source is predominantly dip slip with a dip angle between 20° and 70°. These uncertainties can be removed by introducing the first motion data of long-period P waves.

The body-wave radiation pattern for this earthquake has been studied by *Stauder and Bollinger* [1966]. From P-wave data alone only one nodal plane could be determined unambiguously, as shown in Figure 8. This figure was based on the readings of the long-period seismograms of WWSSN stations and one Japanese station TSK, and is essentially the same as that of Stauder and Bollinger. The P-wave nodal plane has a strike of N43°E dipping 68° toward southeast. If we assume that long-period P waves and surface waves originate from a common source, we can construct a more detailed source model, as follows, by combining

the *P*-wave and surface-wave radiation patterns.

The observation that one nodal line (NE–SW) of the surface-wave radiation patterns nearly coincides with the strike of the *P*-wave nodal plane requires that the source should be almost a pure dip slip; if the source has a significant amount of strike-slip component, the surface-wave nodal line should be rotated with respect to the strike of *P*-wave nodal plane, as we shall see later. Thus the source geometry is constrained to a double-couple pure dip-slip fault, with a strike of N43°E dipping 22° toward northwest (68° towards southeast). The relative excitation and the radiation pattern of the synthetic surface waves for this source model is consistent with the observations as shown in Figures 11 and 12.

Asymmetry. The observed asymmetry of the surface-wave radiation can be explained in terms of the traveling disturbance model as introduced by *Lamb* [1916] and refined by *Ben-Menahem* [1961]. For a precise calculation, the displacement as given by equation 1 or 2 should be integrated over a fault on a sphere with an appropriate rupture velocity and fault length. However, in view of the gross simplifications made in representing the rupture propagation along a fault by the traveling disturbance, it is not meaningful to perform such integrations. In the present paper, the effect of the moving source was included simply by multiplying the Fourier components of the synthetic seismograms by a factor

$$\exp(-ix) \sin x/x$$

$$x = \pi Lf(C/C_0 - \cos\theta_0)/C$$

and inverse-transforming them back to time domain. In the above, L, f, C, C_0, and θ_0 are, respectively, the fault length, frequency, phase velocity of Love or Rayleigh waves of frequency f, rupture velocity, and the azimuth of the station with respect to the direction of the rupture [*Ben-Menahem*, 1961]. By comparing the synthetic seismograms thus calculated with the observed seismograms, we can estimate L and C_0. However, it was found that with the limited frequency band used here it was rather difficult to determine L and C_0 independently. Several examples are illustrated in Figures 9*a*, *b*, *c*, *d*, and *e*. If we assume that $L = 250$ km, we find

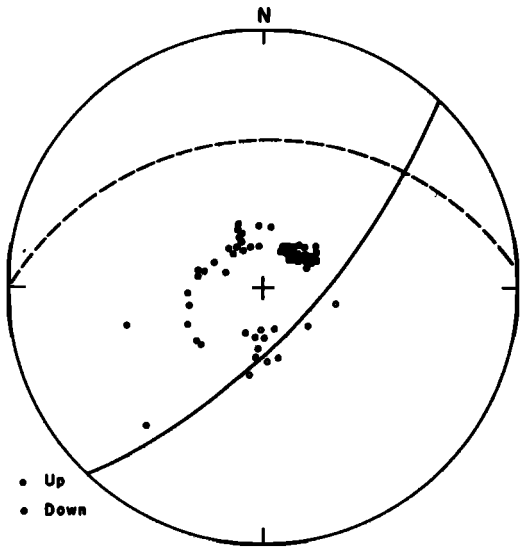

Fig. 8. Stereographic projection (lower hemisphere) of the first motion data of *P* waves. Solid curve is the nodal plane determined from *P*-wave data, and the dashed curve gives the plane *a* of *Stauder and Bollinger* [1966].

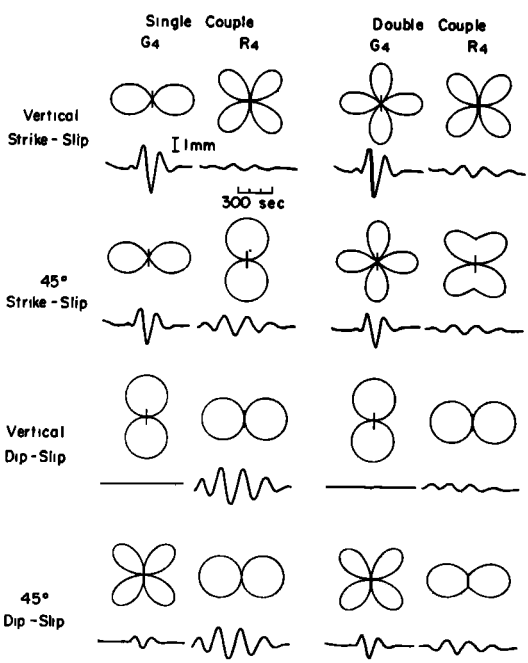

Fig. 7. Radiation pattern (maximum trace amplitude) and relative excitation of Love and Rayleigh waves for eight fundamental source geometries. The wave forms in the loop direction are shown.

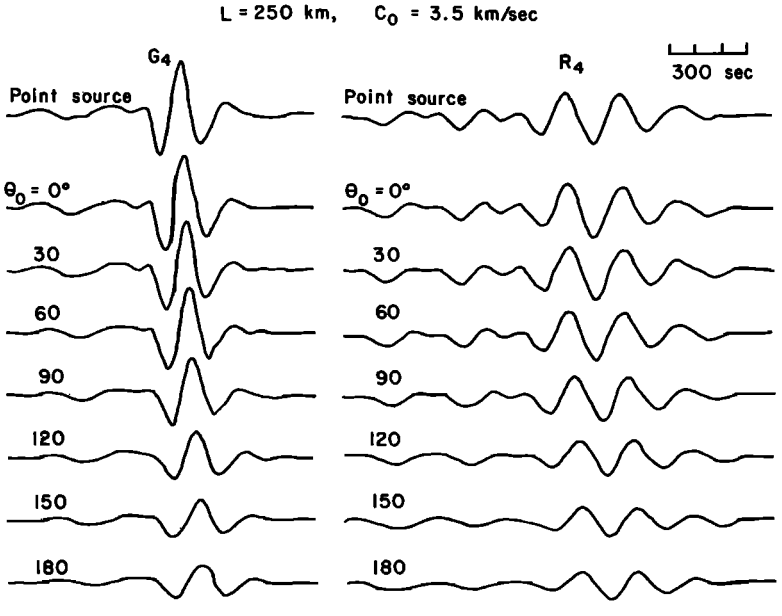

Fig. 9*a*.

Figure 9 shows wave forms of Love and Rayleigh waves for a propagating source with fault length L and rupture velocity C_0. θ_0 is the angle measured from the direction of the rupture propagation.

that $C_0 = 3.5$ km/sec gives the best solution as shown in Figure 9*a*. For this fault length, $C_0 = 2.5$ km/sec gives too large an asymmetry, and $C_0 = 4.5$ km/sec gives too small an asymmetry (see Figures 9*b* and 9*c*). However, for different fault lengths different rupture velocities are more appropriate; as shown in Figures 9*d* and 9*e*, combinations of $L = 300$ km, $C_0 = 4.5$ km/sec and $L = 200$ km, $C_0 = 2.7$ km/sec explain the observed asymmetry equally well. From the dimension of the aftershock area (see Figure 10), it seems most appropriate to take $L = 200$ to 300 km. The rupture velocity can then be estimated to be 2.7 to 4.5 km/sec. In the following discussions, we shall take the middle value, $L = 250$ km and $C_0 = 3.5$ km/sec, but the above uncertainties should be borne in mind. Unless observational data over a wider frequency band are available, more detailed analysis is not meaningful.

Since the observed radiation pattern is nearly symmetric with respect to the strike of the nodal line, the direction of the rupture probably coincides with the strike of the fault. The large amplitude in the northeast direction with respect to the southwest suggests that the rupture started from the southwest end of the focal region and moved toward northeast. This is consistent with the location of the main shock with respect to the aftershock area (Figure 10); the location of the main shock, which is considered to be the starting point of the rupture, is on the southwest end of the aftershock area.

In order to show the over-all agreement between the synthetic and observed seismograms, synthetic seismograms calculated for a reverse dip-slip fault (double couple) with a dip angle of 22°, dip direction of N47°W (strike direction, N43°E), fault length of 250 km, and rupture velocity of 3.5 km/sec are shown in Figures 11 and 12. A step function is assumed for the source-time function. The direction of rupture coincides with the strike of the fault. These synthetic seismograms are computed at a distance of $\pi/2$ and at azimuths corresponding to those of stations used here, so that they can be compared directly with the observed seismograms shown in Figures 1 and 2. From direct comparison of the amplitude, the seismic moment M_0 can be estimated to be 7×10^{28} and

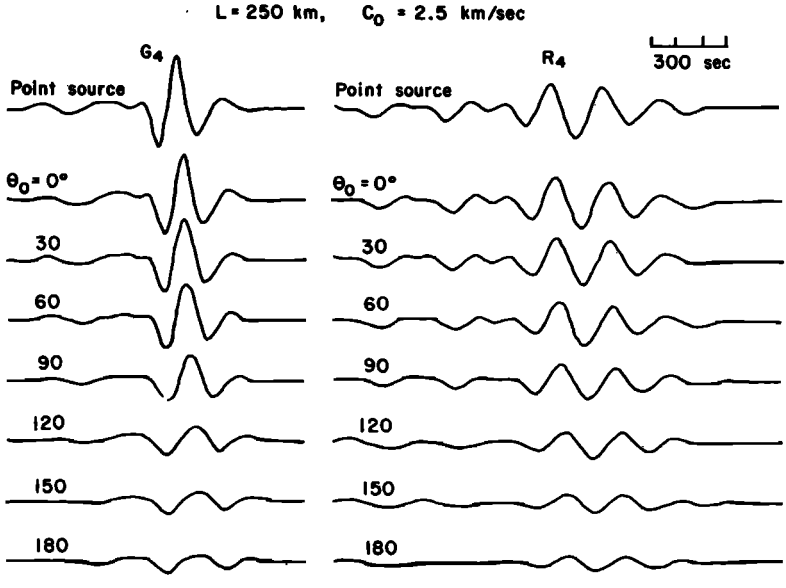

Fig. 9b.

8×10^{28} dyne-cm for Love and Rayleigh waves respectively; the average of 7.5×10^{28} dyne-cm will be used hereafter. K. Abe (article in preparation for publication in *Physics of the Earth and Planetary Interiors*, 1970) estimated the amplitude spectral densities of the free oscillations excited by this earthquake over a period range 300 to 600 sec. According to his estimates, the seismic moment of this earthquake is about 7.5×10^{28} dyne-cm over this period range. This value is consistent with the present result. This agreement suggests that the

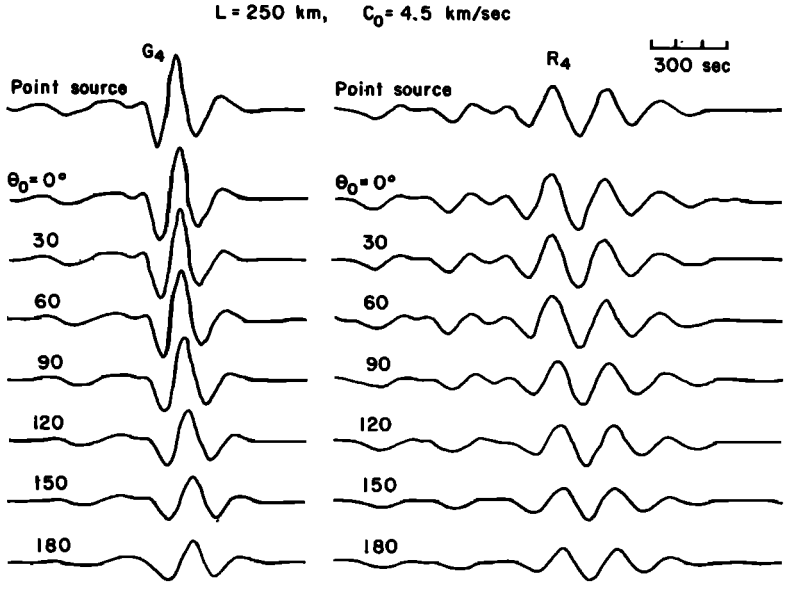

Fig. 9c.

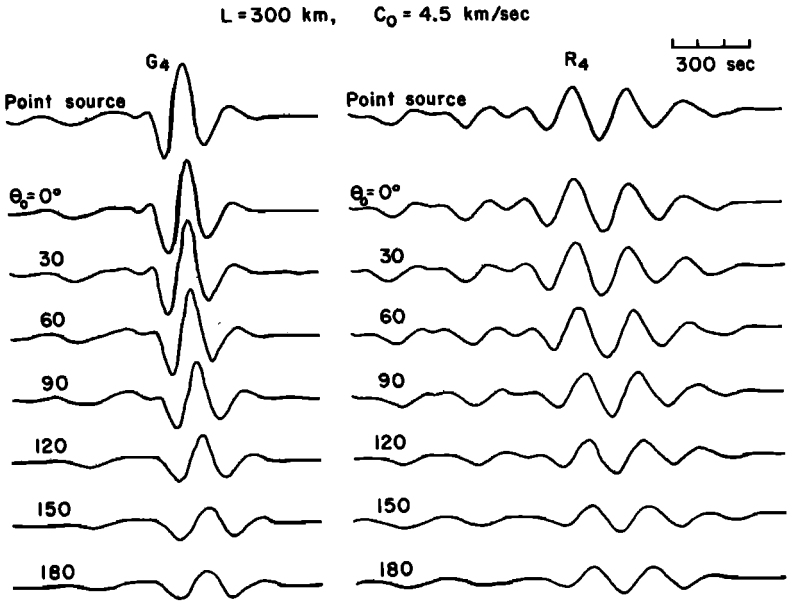

Fig. 9*d*.

assumption of the step source function is reasonable. The close agreement between the synthetic and observed seismograms allows one to say with some confidence that the source model determined here is very reasonable as far as the observed seismological data are concerned.

Phase. It is difficult to use the phase of multiple surface waves for recovering the source phase, as has been pointed out by *Aki* [1962, 1966*a*]. This difficulty is also demonstrated in Figures 1 and 2, where we see that the group arrival times of Love and Rayleigh waves are

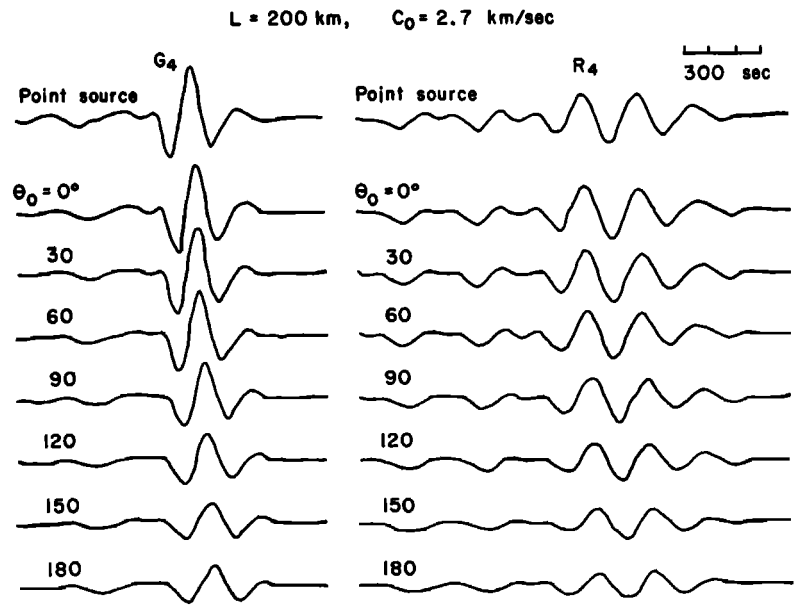

Fig. 9*e*.

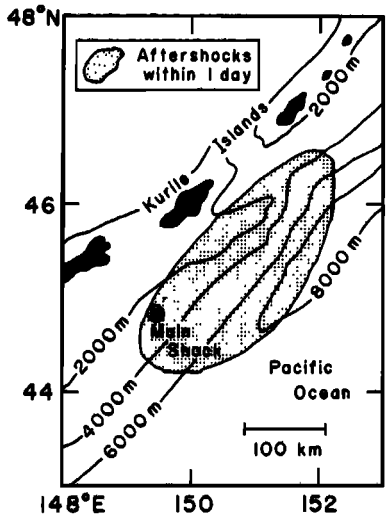

Fig. 10. Aftershock area within one day after the main shock (adopted from *Santô* [1964]).

not so coherent from one station to another as to permit a direct use of the phase for determining the direction of the initial motion at the source.

Since the initial motion of long-period P waves suggests that the source of this earthquake is a reverse fault, the synthetic seismograms have been computed for a reverse fault. If all the assumptions made here are correct, the synthetic seismograms shown in Figures 11 and 12 should be in phase with the observed seismograms shown in Figures 1 and 2. A close inspection reveals that they are nearly in phase except for the stations at azimuths between 90° and 120°. This situation can be more clearly demonstrated in Figure 13, where the difference of the Fourier phase between the synthetic and observed seismograms for several stations is shown. The period is 197 and 183 sec for Rayleigh and Love waves, respectively. The phase difference at $\Delta = \pi/2$ and at 5 hours after origin time is shown for Rayleigh waves and is shown at 4 hours and 15 minutes for Love waves. Although the scatter is fairly large, the difference is within $\pm\pi/2$ at the majority of the stations; this favors the reverse fault. It is found that the stations that show large differences (PRE, NDI, AAE, and SHI for Rayleigh waves; PRE and SHI for Love waves) are located on great circle paths that include the major part of the Himalayas. It is possible that

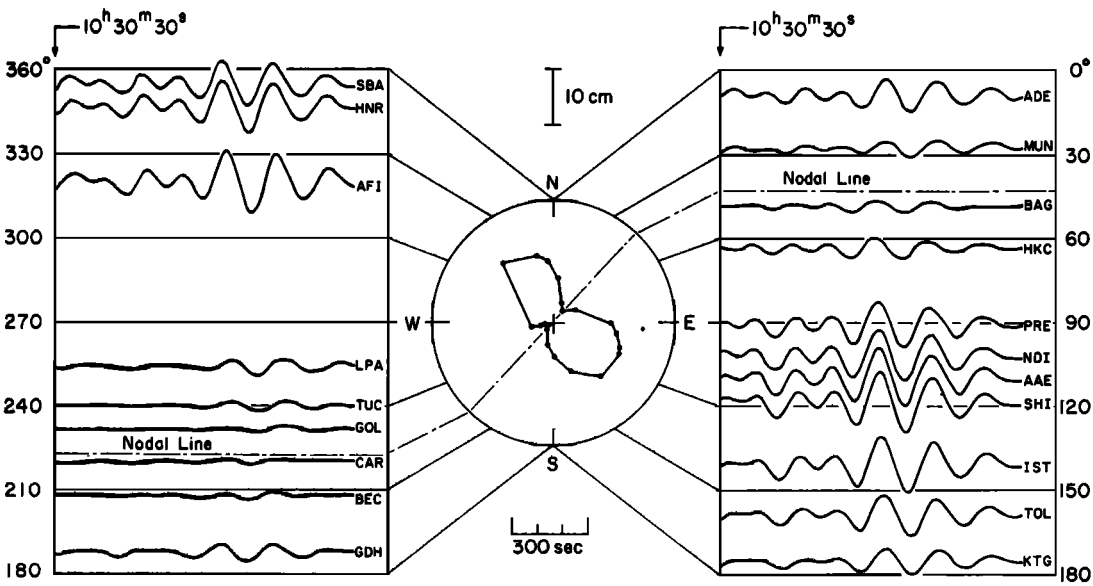

Fig. 11. Synthetic seismograms of Rayleigh waves ($R4$) at a distance of $7\pi/2$. The source is a double-couple dip-slip with a dip angle of 22° and a dip direction of N47°W (strike, N43°E). The fault length is 250 km and the rupture velocity is 3.5 km/sec in the direction N43°E. The source-time function is a step function with a moment of 8×10^{28} dyne-cm. The vertical scale gives the trace amplitude of the standard 30–100 seismograph record with a magnification of 1500.

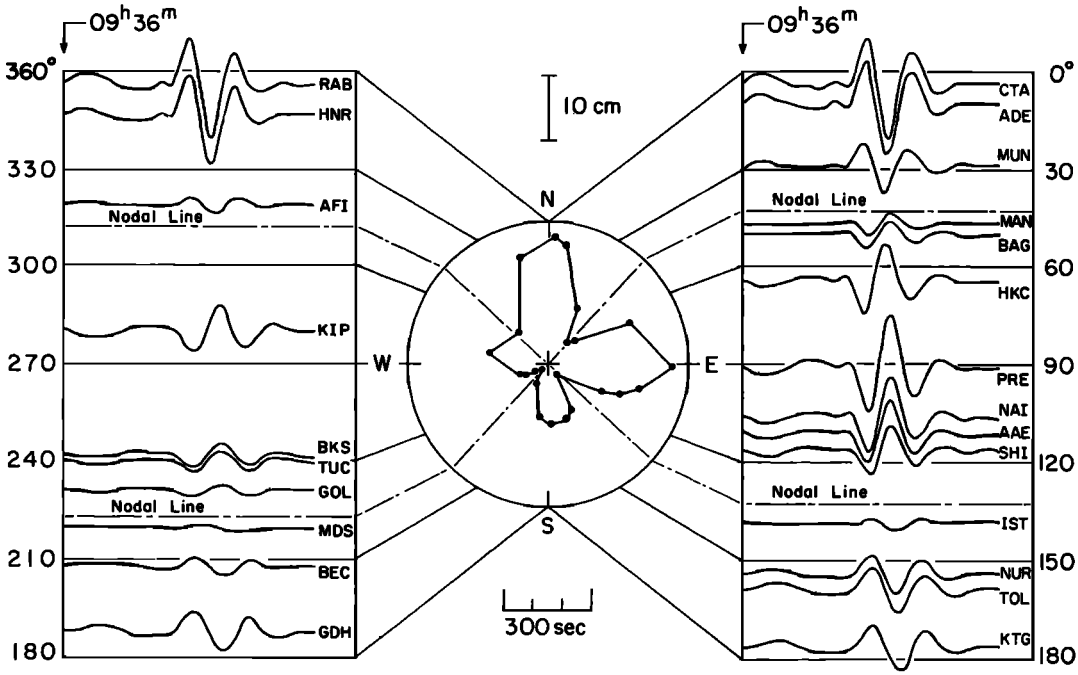

Fig. 12. Synthetic seismograms of Love waves (*G*4). The moment is 7×10^{28} dyne-cm. (For other parameters, see the caption for Figure 11).

for these paths the phase has been greatly disturbed by a large structural heterogeneity beneath the Himalayas. By and large, the reverse fault seems to be evidenced, though marginal, by the surface-wave data.

Discussion and Conclusions

Stauder and Bollinger [1966] determined source parameters for this earthquake using the first motions of *P* waves and the polarization angles of *S* waves. Their solutions are (see also Figure 8): plane *a*, dip direction 357°, dip 30°, slip angle 50°; plane *b*, dip direction 133°, dip 68°, slip angle 69°. It is worthwhile to compare the radiation patterns of surface waves for their model with the observed radiation patterns. Figure 14 shows the comparison. Since the solution by Stauder and Bollinger has a considerable amount of strike-slip component, the nodal lines of the surface-wave radiation patterns are rotated with respect to the body-wave nodal lines, and the Love wave excitation is augmented. The surface-wave radiation pattern for this model does not seem so consistent as the present solution, 22° pure dip-slip. This disagreement can be attributed to two causes: (1) the fault motion associated with the body-wave radiation may be slightly different from that associated with the surface-wave radiation; (2) the use of *S* waves is very difficult for such a large earthquake, and the parameters for plane *a* can be subject to large uncertainty (Stauder, personal communication). In view of these, we do not consider the body-wave results incompatible with the surface-wave results.

Since the seismic moment Mo and approximate fault dimensions have been determined, the average slip displacement $\bar{u}$ along the fault, stress drop σ, strain drop ϵ, and the released strain energy W can be readily estimated according to the slip dislocation theory of faults [see *Aki*, 1966*b*]. The formulas used here are:

$$\bar{u} = Mo/\mu S \qquad \sigma = \frac{16}{3\pi}\mu\bar{u}/w$$

$$\epsilon = \sigma/\mu \qquad W = \frac{4}{\pi}\frac{\mu(\lambda+\mu)}{(\lambda+2\mu)}\bar{u}^2 L$$

where μ is rigidity, λ is Lamé constant, S is the area of the fault surface, w, the width of the

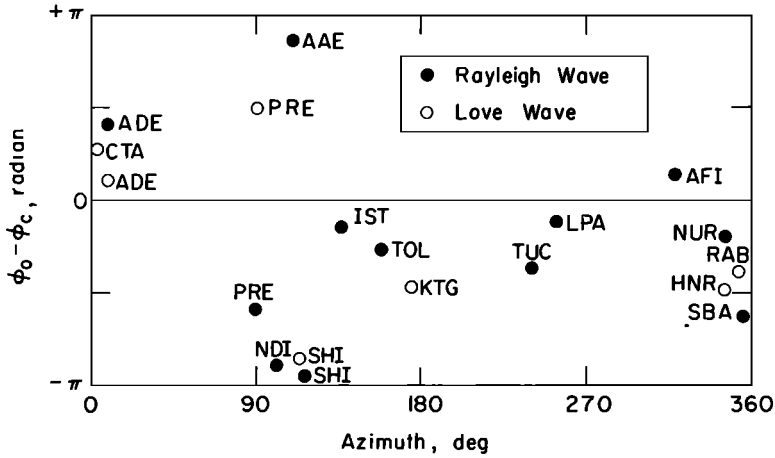

Fig. 13. The difference of the phase between observed (ϕ_o) and synthetic (ϕ_c) seismograms.

fault perpendicular to its strike, and L, the length of the fault in the direction of its strike. Using the values $Mo = 7.5 \times 10^{28}$ dyne-cm, $w = 150$ km, $L = 250$ km, $S = 3.75 \times 10^4$ km^2, $\lambda = \mu = 0.7 \times 10^{12}$ dyne-cm^{-2}, we have $\bar{u} \sim 3$ meters, $\sigma \sim 23$ bars, $\epsilon \sim 0.32 \times 10^{-4}$, and $W \sim 1.2 \times 10^{24}$ ergs. These values are subject to some uncertainty because of the gross simplification made in the dislocation model of the fault. However, since no geodetic observations could be made for this earthquake, we consider that these are the most reliable estimates that currently available geophysical technique can provide.

The actual fault plane can be either a plane dipping 22° toward northwest or a plane dipping 68° toward southeast. From the radiation pattern, it is not possible to determine on which one of these planes the actual displacemen took place. However, considering the shallow depths and a relatively large lateral breadth of the aftershock activity [*Santô*, 1964], the plane dipping 22° toward northwest seems preferable for the fault plane. If this is the case, the present solution suggests an underthrusting motion of an oceanic block beneath a continental block. If a recurrence time of about 100 years is assumed for major earthquakes in this region, the average displacement of 3 meters estimated above suggests a time-average slip rate of 3 cm/year in this region. This picture matches the current sea-floor spreading hypothesis reasonably well. *Le Pichon* [1968] estimated the rate of the differential movement of lithosphere from magnetic data at about 8 cm/year for the Kurile region. *Brune* [1968] estimated the average slip rate for major fault zones from accumulated seismic moment, and obtained the values 15.7 and 3.8 cm/year for Japan and Aleutians respectively.

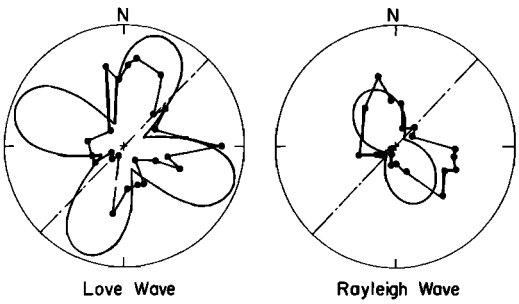

Fig. 14. Surface-wave radiation patterns for *Stauder and Bollinger* [1966] model as compared with the observed radiation patterns.

It can be concluded that synthetic seismograms calculated for an improved earth model can be used for a most straightforward interpretation of surface-wave data of great earthquakes. The source parameters of the Kurile Islands earthquake of October 13, 1963, determined by this technique, are as follows:

Source geometry, double-couple reverse dip slip.
Strike, N43°E.
Dip, 22°NW (68°SE).
Fault length, 200 to 300 km.
Rupture velocity, 2.7 to 4.5 km/sec toward northeast.

Source-time function, step function.
Seismic moment, 7.5×10^{28} dyne-cm.
Average slip, 3 meters.
Stress drop, 23 bars.
Strain drop, 0.32×10^{-4}.
Released strain energy, 1.2×10^{24} ergs.

Acknowledgments. I benefited from discussions with Masanori Saito and Katsuyuki Abe in the early stages of this work. Dr. W. Stauder kindly provided me with some unpublished information for this earthquake. I am grateful to Frank Press for generously making available to me, in advance of publication, his new earth models, by which the synthetic seismograms were greatly improved. I thank Keiiti Aki and Frank Press who kindly read the manuscript and made many valuable suggestions. I am indebted to Tomowo Hirasawa for the interpretation of the body-wave solution, and to Ralph Wiggins for the construction of the earth model used here.

This work was partially supported by the Air Force Office of Scientific Research under contract AF49 (638) 1632.

References

Aki, K., Study of earthquake mechanism by a method of phase equalization applied to Rayleigh and Love waves, *J. Geophys. Res., 65,* 729, 1960*a*.

Aki, K., Further study of the mechanism of circum-Pacific earthquakes from Rayleigh waves, *J. Geophys. Res., 65,* 4165, 1960*b*.

Aki, K., Accuracy of the Rayleigh wave method for studying the earthquake mechanism, *Bull. Earthquake Res. Inst. Tokyo Univ., 40,* 91, 1962.

Aki, K., Generation and propagation of *G* waves from the Niigata earthquake of June 16, 1964, 1, A statistical analysis, *Bull. Earthquake Res. Inst. Tokyo Univ., 44,* 23, 1966*a*.

Aki, K., Generation and propagation of *G* waves from the Niigata earthquake of June 16, 1964, 2, Estimation of earthquake moment, released energy, and stress-strain drop from the *G*-wave spectrum, *Bull. Earthquake Res. Inst. Tokyo Univ., 44,* 73, 1966*b*.

Alterman, Z., H. Jarosch, and C. L. Pekeris, Oscillations of the earth, *Proc. Roy. Soc. London A, 252,* 80, 1959.

Benioff, H., F. Press, and S. Smith, Excitation of the free oscillations of the earth by earthquakes, *J. Geophys. Res., 66,* 605, 1961.

Ben-Menahem, A., Radiation of seismic surface waves from finite moving sources, *Bull. Seismol. Soc. Amer., 51,* 401, 1961.

Ben-Menahem, A., and D. G. Harkrider, Radiation patterns of seismic surface waves from buried dipolar point sources in a flat stratified earth, *J. Geophys. Res., 69,* 2605, 1964.

Ben-Menahem, A., and M. N. Toksöz, Source mechanism from spectra of long-period seismic surface waves, 1, The Mongolian earthquake of December 4, 1957, *J. Geophys. Res., 67,* 1943, 1962.

Ben-Menahem, A., and M. N. Toksöz, Source mechanism from spectrums of long-period surface waves, 2, The Kamchatka earthquake of November 4, 1952, *J. Geophys. Res., 68,* 5207, 1963*a*.

Ben-Menahem, A., and M. N. Toksöz, Source mechanism from spectra of long-period seismic surface waves, 3, The Alaska earthquake of July 10, 1958, *Bull. Seismol. Soc. Amer., 53,* 905, 1963*b*.

Bolt, B., and J. Dorman, Phase and group velocities of Rayleigh waves in a spherical, gravitating earth, *J. Geophys. Res., 66,* 2965, 1961.

Brune, J., Radiation pattern of Rayleigh waves from the southeast Alaska earthquake of July 10, 1958, *Publ. Dominion Astrophys. Observ., Ottawa, 24,* 373, 1961.

Brune, J., Correction of initial phase measurements for the southwest Alaska earthquake of July 10, 1958, and for certain nuclear explosions, *J. Geophys. Res., 67,* 3643, 1962.

Brune, J. N., Seismic moment, seismicity, and rate of slip along major fault zones, *J. Geophys. Res., 73,* 777, 1968.

Brune, J. N., J. Nafe, and J. Oliver, A simplified method for the analysis and synthesis of dispersed wave trains, *J. Geophys. Res., 65,* 287, 1960.

Hagiwara, T., A note on the theory of the electromagnetic seismograph, *Bull. Earthquake Res. Inst. Tokyo Univ., 36,* 139, 1958.

Haskell, N. A., Radiation pattern of Rayleigh waves from a fault of arbitrary dip and direction of motion in a homogeneous medium, *Bull. Seismol. Soc. Amer., 53,* 619, 1963.

Haskell, N. A., Radiation pattern of surface waves from point sources in a multi-layered medium, *Bull. Seismol. Soc. Amer., 54,* 377, 1964.

Jobert, N., Excitation des oscillations propres de torsion de la terre, *Ann. Geophys., 18,* 372, 1962.

Kanamori, H., Velocity and *Q* of mantle waves, *Phys. Earth Planet. Interiors, 2,* in press, 1970.

Kanamori, H., and K. Abe, Deep structure of island arcs as revealed by surface waves, *Bull. Earthquake Res. Inst. Tokyo Univ., 46,* 1001, 1968.

Lamb, H., On the propagation of tremors over the surface of an elastic solid, *Phil. Trans. Roy. Soc. London A, 203,* 1, 1904.

Lamb, H., On waves due to a traveling disturbance, with an application to waves in superposed fluids, *Phil. Mag., 13*(6), 386, 1916.

Le Pichon, X., Sea-floor spreading and continental drift, *J. Geophys. Res., 73,* 3661, 1968.

Press, F., Earth models consistent with geophysical data, *Phys. Earth Planet. Interiors, 3,* 3, 1970.

Press, F., A. Ben-Menahem, and M. N. Toksöz, Experimental determination of earthquake fault length and rupture velocity, *J. Geophys. Res., 66,* 3471, 1961.

Saito, M., Excitation of free oscillations and surface waves by a point source in a vertically heterogeneous earth, *J. Geophys. Res., 72,* 3689, 1967.

Santô, T., Shock sequences of the southern Kurile Islands from October 9 to December 31, 1963, *Bull. Int. Inst. Seismol. Earthquake Eng., 1,* 33, 1964.

Satô, Y., and T. Usami, Basic study on the oscillation of a homogeneous elastic sphere, 1, 2, 3, *Geophys. Mag., 31,* 15, 1962.

Satô, Y., T. Usami, and M. Ewing, Basic study on the oscillation of a homogeneous elastic sphere, 4, *Geophys. Mag., 31,* 237, 1962.

Satô, Y., T. Usami, and M. Landisman, Theoretical seismograms of spheroidal type on the surface of a gravitating elastic sphere, 2, Case of Gutenberg-Bullen *A'* earth model, *Bull. Earthquake Res. Inst. Tokyo Univ., 45,* 601, 1967.

Satô, Y., T. Usami, and M. Landisman, Theoretical seismograms of torsional disturbances excited at a focus within a heterogeneous spherical earth—Case of a Gutenberg-Bullen *A'* earth model, *Bull. Seismol. Soc. Amer., 58,* 133, 1968.

Stauder, W., and G. A. Bollinger, The *S*-wave project for focal mechanism studies, earthquakes of 1963, *Bull. Seismol. Soc. Amer., 56,* 1363, 1966.

Takeuchi, H., M. Saito, and N. Kobayashi, Study of shear velocity distribution in the upper mantle by mantle Rayleigh and Love waves, *J. Geophys. Res., 67,* 2831, 1962.

Tsai, B., and K. Aki, Simultaneous determination of the seismic moment and attenuation of seismic surface waves, *Bull. Seismol. Soc. Amer., 59,* 275, 1969.

Usami, T., Y. Satô, and M. Landisman, Theoretical seismograms of spheroidal type on the surface of a heterogeneous spherical earth, *Bull. Earthquake Res. Inst. Tokyo Univ., 43,* 641, 1965.

Wu, F., and A. Ben-Menahem, Surface-wave radiation pattern and source mechanism of the September 1, 1962, Iran earthquake, *J. Geophys. Res., 70,* 3943, 1965.

(Received January 12, 1970.)